LETTER

doi:10.1038/nature11792

# Mitotic cell rounding accelerates epithelial invagination

Takefumi Kondo[1] & Shigeo Hayashi[1,2]

**Mitotic cells assume a spherical shape by increasing their surface tension and osmotic pressure by extensively reorganizing their interphase actin cytoskeleton into a cortical meshwork and their microtubules into the mitotic spindle[1,2]. Mitotic entry is known to interfere with tissue morphogenetic events that require cell-shape changes controlled by the interphase cytoskeleton, such as apical constriction[3–5]. However, here we show that mitosis plays an active role in the epithelial invagination of the *Drosophila melanogaster* tracheal placode. Invagination begins with a slow phase under the control of epidermal growth factor receptor (EGFR) signalling; in this process, the central apically constricted cells, which are surrounded by intercalating cells[6,7], form a shallow pit. This slow phase is followed by a fast phase, in which the pit is rapidly depressed, accompanied by mitotic entry, which leads to the internalization of all the cells in the placode. We found that mitotic cell rounding, but not cell division, of the central cells in the placode is required to accelerate invagination, in conjunction with EGFR-induced myosin II contractility in the surrounding cells. We propose that mitotic cell rounding causes the epithelium to buckle under pressure and acts as a switch for morphogenetic transition at the appropriate time.**

The invagination of epithelial placodes converts flat sheets into the three-dimensional structures that form complex organs, and it is a key morphogenetic process in animal development[8]. A major mechanism of invagination is apical constriction, which is driven by actomyosin contraction[9]. However, not all constricted cells invaginate[10,11], and some cell internalization occurs without apical constriction[6,7,12,13], suggesting that additional mechanisms of inward cell movement contribute to invagination.

To obtain three-dimensional information about cell behaviour during invagination, we performed live imaging of the *Drosophila* tracheal placode. Ten pairs of tracheal placodes, each of which is composed of about 40 cells, are formed in the ectoderm at mid-embryogenesis, and each placode initiates invagination simultaneously[14]. Using an adherens junction marker, DE-cadherin–green fluorescent protein (E-cad–GFP)[15], we found that the adherens junctions of the central placode cells slowly created a depression by apical constriction, which became the tracheal pit[7] (Fig. 1a). After 30 to 60 min of slow movement (slow phase), the tracheal pit was suddenly enlarged, and the tracheal cells were rapidly internalized (fast phase) and eventually formed L-shaped tube structures (Fig. 1a, b, e, Supplementary Fig. 1 and Supplementary Video 1).

After the fast transition, all the tracheal cells and surrounding epidermal cells entered mitosis 16, the final round of embryonic mitosis[16]. We noticed that the fast invagination was always associated with the mitotic entry of central cells that were frequently the first to enter mitosis 16 (10 out of 14 cases) (Fig. 1b, c and Supplementary Fig. 1a). Intriguingly, mitotic rounding of the central constricted cells occurred simultaneously with the rapid depression of their apices, followed by chromosome condensation 10 min later (Fig. 1d and Supplementary Video 2). In this study, we call this atypical mitotic rounding associated with apical depression 'internalized cell rounding', to distinguish it from canonical surface mitosis (surface cell rounding).

To determine whether cell rounding is required for invagination, we analysed zygotic mutants of the cell-cycle gene *Cyclin A* (*CycA*), which fail to enter mitosis 16 (ref. 17), and *double parked*$^{a3}$ (*dup*$^{a3}$), which show a prolonged S phase 16 and delayed entry into mitosis 16 (ref. 18). Tracheal invagination was initiated normally in the *CycA* and *dup*$^{a3}$ mutants, but proceeded more slowly than in controls (Fig. 2a, d, Supplementary Fig. 2 and Supplementary Video 3), indicating that entry into mitosis 16 is required for proper timing of the fast phase.

Although delayed, the accelerated invagination in the *CycA* or *dup*$^{a3}$ mutants eventually occurred, allowing the formation of tube structures (Fig. 2d and Supplementary Fig. 2b) and suggesting that additional mechanisms are involved. After invagination, fibroblast growth factor (FGF) signalling is activated in the tracheal cells to induce branching morphogenesis through chemotaxis[19,20]. To examine the contribution of FGF signalling to invagination, we analysed mutants of the FGF ligand *branchless* (*bnl*) or the FGF receptor *breathless* (*btl*) (Fig. 2b, e and Supplementary Fig. 3a, c). These mutants invaginated normally, indicating that chemoattraction to FGF is dispensable for invagination.

Next, to assess FGF's role in the mitosis-defective condition, we analysed double mutants for *CycA* and *bnl* or *CycA* and *btl*, and found that they showed slower invagination than *CycA* single mutants (Fig. 2c, f and Supplementary Fig. 3b, d). Furthermore, the invagination in these double mutants was incomplete, in that the cells failed to form L-shaped tubular structures (Fig. 2c, Supplementary Fig. 3b and Supplementary Video 4, see 120-min time point). Therefore, FGF signalling is critical for invagination when mitosis is blocked, serving a back-up role. Tracheal-specific *CycA* expression rescued the defects in invagination speed and tube structure in the *CycA btl* mutants (Supplementary Fig. 4). In addition, we occasionally observed mitosis of cells outside the pit that occurred before the mitosis of the central apically constricted cells and was not correlated with the fast invagination phase (Supplementary Fig. 1c). Thus, mitosis of the surrounding epidermal cells is dispensable for tracheal invagination. Taken together, we conclude that mitotic entry of central cells is a major mechanism for accelerating tracheal invagination.

To distinguish the role of cell rounding from that of cell division in the fast phase, we used the microtubule inhibitor colchicine to arrest the cell cycle after cell rounding. Colchicine treatment after mitosis 15 induced M-phase arrest at mitosis 16, but the fast invagination movement accompanied by cell rounding was not affected (Fig. 3 and Supplementary Video 5). This result indicates that cell rounding, but not cell division, is responsible for the acceleration phase of the tracheal invagination.

Mitosis of cells in the columnar epithelium normally occurs at the apical surface after surface rounding[21,22]. We next asked how the apical surface of the central cells becomes depressed during internalized cell rounding. One possible model explains internalized cell rounding as

[1]Laboratory for Morphogenetic Signaling, RIKEN Center for Developmental Biology, 2-2-3, Minatojima-Minamimachi, Chuo-ku, Kobe, Hyogo 650-0047, Japan. [2]Department of Biology, Kobe University Graduate School of Science, Kobe, Hyogo 657-8501, Japan.

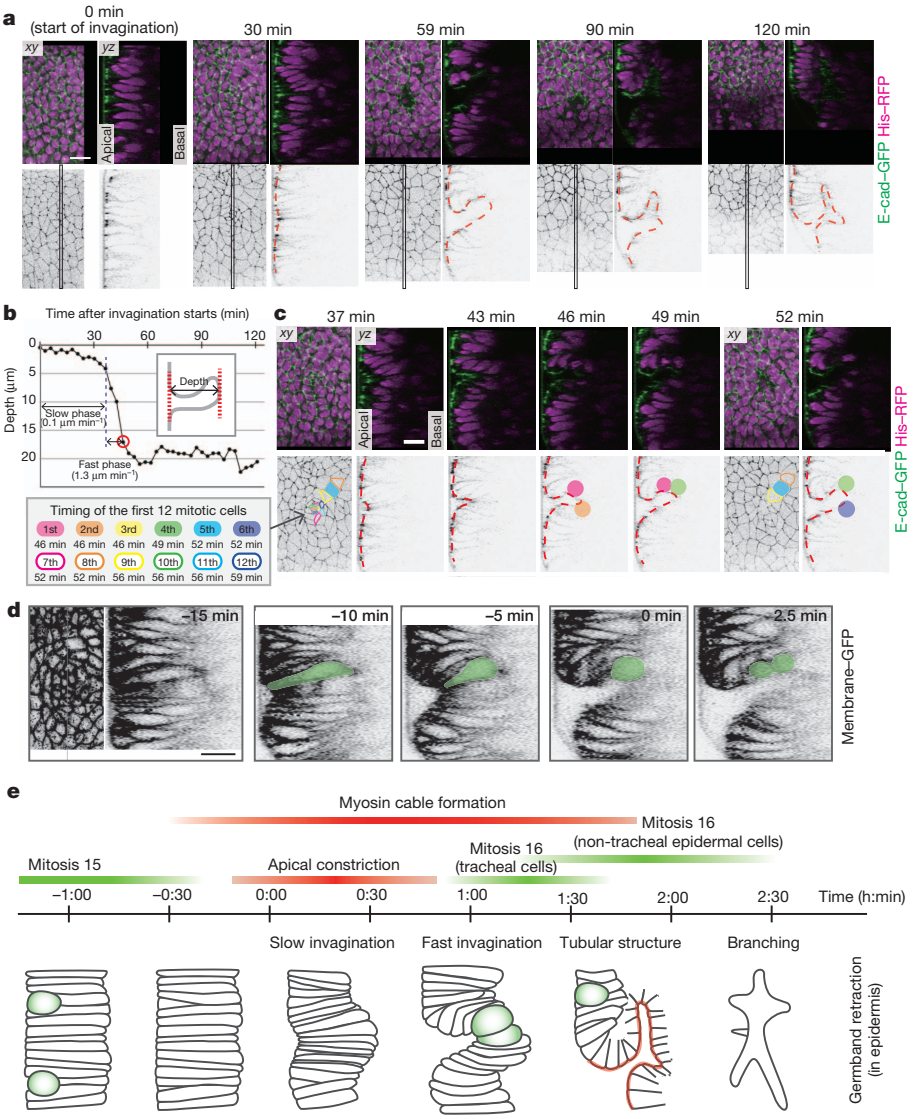


**Figure 1 | Two-step process of tracheal invagination.** **a**, Time-lapse images of E-cad–GFP (green) and histone H2Av–red fluorescent protein (His–RFP) (magenta) during tracheal invagination. Red dashed lines outline the adherens junctions. Time zero was the initiation of adherens junction depression. **b**, Time course of pit-depth change measured for the images in **a**. Red circle indicates the timing of the first appearance of condensed chromosomes (46 min in **c**). **c**, Time-lapse images of the fast transition. The first 12 mitotic cells are coloured as shown. **d**, Time-lapse images of GFP-CAAX (membrane–GFP). Cells that became spherical are coloured green. Time zero was defined by the complete mitotic rounding of the green cell. **e**, Schematic of tracheal invagination. Scale bars, 10 μm.

cell-autonomously controlled by the association of the cells with the basement membrane or underlying mesodermal cells. However, genetic removal of basement-membrane adhesion by the maternal and zygotic mutation of *βPS-integrin* (also known as *mys*)[23] did not compromise the speed of invagination, and *snail twist* double-mutant embryos, which lack mesodermal cells[24], still showed tracheal invagination with internalized cell rounding (Supplementary Fig. 5). These results suggest that anchoring to the basal side is probably not required.

A second model proposes that the apical depression of the rounding cells is driven by local planar interactions among the tracheal cells. Before and during tracheal invagination, myosin II is enriched at the cell boundaries tangential to the centre of the placode and regulates cell intercalation[7] (Supplementary Fig. 6a). We noted that the myosin II level in the central cells was lower than in the surrounding, intercalating cells (Supplementary Fig. 6a, compare to myosin II distribution in the ventral furrow in Supplementary Fig. 6c). Nevertheless, the apices of the central cells were constricted during the slow phase (Supplementary Fig. 6b), strongly suggesting that the surrounding cells exerted centripetal pressure on the central cells through myosin II cables[7]. Myosin II cables fail to form in EGFR signalling mutants (such as *rho*, the rhomboid endopeptidase required for EGF ligand maturation, and *Egfr*), and apical constriction is impaired in these mutants[6,7]. The first few cells undergoing mitosis 16 in the tracheal placode of *rho* or *Egfr* mutants showed surface cell rounding with expanded apices (Supplementary Figs 7 and 8b), indicating that EGFR signalling is required to couple the mitotic cell rounding with fast apical depression. We speculate that the columnar shape of the central cells resists centripetal movements, resulting in the accumulation of inward pressure during the slow phase. The existence of such resistance was supported by the results of a physical perturbation experiment using a pulsed ultraviolet laser (Supplementary Fig. 9, Supplementary Videos 7–9, and Supplementary Notes). The cell rounding associated with mitotic entry would release the stored inward pressure by means of cytoskeletal remodelling that causes rapid depression of apical surface together with the active shortening of cell height, leading to rapid buckling of the apical surface and the fast phase of invagination (Fig. 4m and Supplementary Fig. 10a).

Even with the loss of both EGFR and FGF signalling, the tracheal placodes form moderately invaginated structures[6] (Fig. 4e–h,

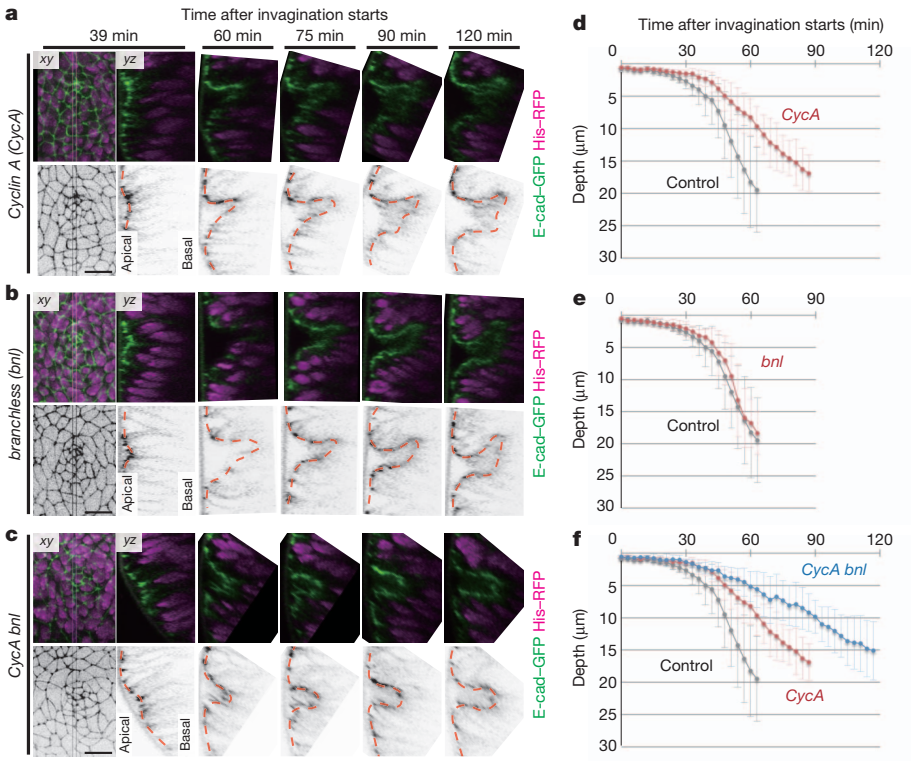


**Figure 2 | Mitosis is required for the acceleration of invagination.** **a–c**, Time-lapse images of tracheal invagination in *CycA* (**a**), *bnl* (**b**) and *CycA bnl* (**c**) mutants carrying E-cad–GFP (green) and His–RFP (magenta). **d–f**, Depth of tracheal pits in the mutants and control. Error bars indicate s.d. (control: $n = 14$; *CycA*: $n = 9$; *bnl*: $n = 8$; and *CycA bnl*: $n = 7$). Scale bars, 10 μm.

Supplementary Fig. 8d and Supplementary Video 6), compared to the flat tracheal placode observed in the *rho bnl CycA* triple mutant at the same stage (Fig. 4i–l and Supplementary Video 10), indicating that cells needed to undergo mitosis 16 to induce invagination, independent of EGFR and FGF signalling. In *rho bnl* double mutants, although the cells undergoing the earliest mitoses showed surface cell rounding (Fig. 4f), some of the subsequent mitotic events were coupled to apical depression and internalized cell rounding (Fig. 4g), and invaginated structures eventually appeared (Fig. 4h and Supplementary Video 6). Unlike the earlier mitotic events on the surface, the internalized rounding cells in the *rho bnl* embryos showed constricted apices and were surrounded by apically rounded cells before mitosis (Supplementary Fig. 8b). Internalized rounding with a constricted apical surface were shared properties of cells in mitoses leading to invagination, in both control and *rho bnl* embryos (Supplementary Fig. 8c). We suggest that the first few cells undergoing surface cell rounding compress the adjacent interphase cells and restrict their apical area, so that they are forced to move internally after rounding, causing the epithelial layer to buckle and invaginate.

Although invagination was largely blocked in the *rho bnl CycA* triple mutants, any double mutant combination permitted invagination to some degree (Figs 2 and 4 and Supplementary Figs 3, 8 and 11), indicating that three qualitatively distinct mechanisms, mitotic cell rounding, myosin II contractility (EGFR) and active cell motility (FGFR), can independently trigger invagination (Supplementary Fig. 11m and Supplementary Notes). In the normal context of wild-type development the combination of cell rounding and EGFR signalling may optimize the timing and speed of invagination, and then

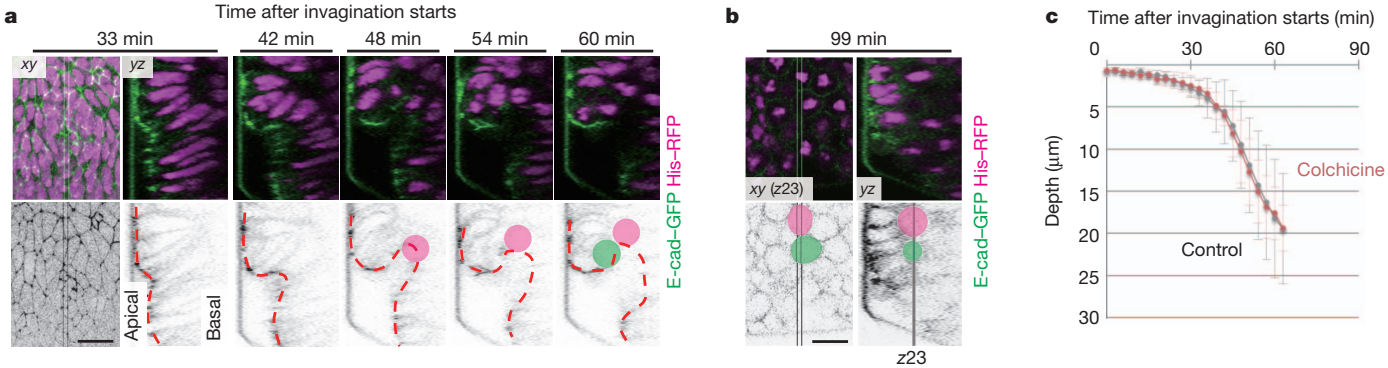


**Figure 3 | Mitotic cell rounding is sufficient for the fast transition.** **a–b**, Time-lapse images of tracheal invagination in a colchicine-treated embryo with E-cad–GFP (green) and His–RFP (magenta). The first rounding cell is coloured magenta, and an additional rounding cell is coloured green. In **b**, *z*23 indicates single plane at the *z* section 23 from the top. **c**, Mean pit depth of the colchicine-treated tracheal invagination. Error bars indicate s.d. (control: $n = 14$ and colchicine: $n = 8$). Although almost all the cells arrested at the M phase and the epithelial structure were eventually disrupted (**b**), the tracheal placodes invaginated normally (**c**) with cell rounding identical to those of controls (**a**). Scale bar, 10 μm.

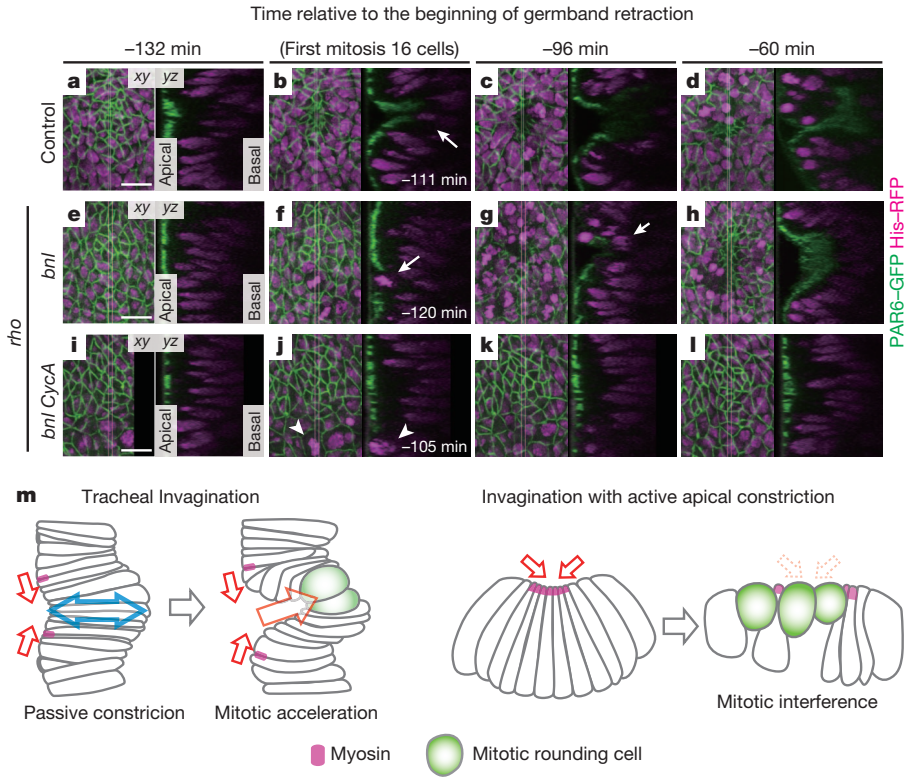


**Figure 4 | Mitosis triggers invagination independent of EGF and FGF signalling.** **a**–**l**, Time-lapse images of tracheal placode in control (**a**–**d**), *rho bnl* (**e**–**h**) and *rho bnl CycA* (**i**–**l**) embryos with PAR-6–GFP, which labels the subapical region, and His–RFP (magenta). Time zero is the initiation of germband retraction. Arrows indicate mitotic cells. Arrowheads in **j** indicate delayed mitosis 15. **m**, Model for tracheal invagination with mitotic rounding (left). Mitotic cell rounding releases the resistance of central cells (blue arrow) to centripetal forces (red arrows) as the cells shorten, leading to rapid epithelial buckling (large red arrow). In the model (right) of invagination with active apical constriction (red arrows above constricted cells labelled with magenta), mitotic entry interferes with invagination owing to the disappearance of inward forces (red dashed arrows). See Supplementary Fig. 10 for details. Scale bars, 10 μm.

invaginated tracheal sacs subsequently respond to FGF emanating from several target tissues guiding branching morphogenesis.

Our observations demonstrates a new role for mitosis in tissue morphogenesis to generate mechanical force through cell rounding, independent of cell division. This is distinct from previously described invagination mechanisms involving cell-autonomous constriction by the apical activation of actomyosin contractility[25,26], which is incompatible with mitosis[3–5] (Fig. 4m and Supplementary Fig. 10). Mitosis 16 outside the tracheal placode occurs in clusters on the ectoderm surface, but does not lead to invagination, suggesting that the tracheal placode is sensitized to invaginate upon mitosis, independent of EGFR and FGFR signalling. Future research to uncover the properties of the tracheal placode that enables it to respond to clustered mitosis will explain not only this new mode of morphogenesis, but also the homeostasis mechanisms of epithelial architecture.

## METHODS SUMMARY

*Drosophila* eggs were collected at 25 °C. Dechorionated embryos were mounted on a glass-bottomed dish (IWAKI) with glue and covered with water. Fluorescent images were captured by a confocal laser-scanning microscope (Olympus FV1000 with 15 mW laser diode 473 nm and 15 mW laser diode 559 nm lasers) with a ×60 oil immersion objective (PLAPON 60XO, numerical aperture 1.42, Olympus) at 25 °C, until the initiation of germband retraction (end of stage 11). All the acquired images were smoothed with a 1-pixel-radius median filter and a 1-pixel full-width at half-maximum Gaussian filter, and movements along the *x*–*y* position between time points were corrected by iSEMS[27]. The *y*–*z* or *x*–*z* projected views were generated by software developed by K. Kato (unpublished software). The apical area and depth of the apical surface were measured using Image J and calculated with Microsoft Excel.

Detailed information about the reagents and methods used in this paper, including the *Drosophila* stocks, live imaging, laser ablation, image processing, plasmid construction, drug treatment and immunohistochemistry is included in the Methods.

**Full Methods** and any associated references are available in the online version of the paper.

**Received 11 May; accepted 13 November 2012.**
**Published online 13 January 2013.**

1. Théry, M. & Bornens, M. Get round and stiff for mitosis. *HFSP J.* **2,** 65–71 (2008).
2. Stewart, M. P. *et al.* Hydrostatic pressure and the actomyosin cortex drive mitotic cell rounding. *Nature* **469,** 226–230 (2011).
3. Großhans, J. & Wieschaus, E. A genetic link between morphogenesis and cell division during formation of the ventral furrow in *Drosophila*. *Cell* **101,** 523–531 (2000).
4. Mata, J., Curado, S., Ephrussi, A. & Rørth, P. Tribbles coordinates mitosis and morphogenesis in *Drosophila* by regulating String/CDC25 proteolysis. *Cell* **101,** 511–522 (2000).
5. Seher, T. C. & Leptin, M. Tribbles, a cell-cycle brake that coordinates proliferation and morphogenesis during *Drosophila* gastrulation. *Curr. Biol.* **10,** 623–629 (2000).
6. Brodu, V. & Casanova, J. The RhoGAP *crossveinless*-c links *trachealess* and EGFR signaling to cell shape remodeling in *Drosophila* tracheal invagination. *Genes Dev.* **20,** 1817–1828 (2006).
7. Nishimura, M., Inoue, Y. & Hayashi, S. A wave of EGFR signaling determines cell alignment and intercalation in the *Drosophila* tracheal placode. *Development* **134,** 4273–4282 (2007).
8. Lecuit, T. & Lenne, P.-F. Cell surface mechanics and the control of cell shape, tissue patterns and morphogenesis. *Nature Rev. Mol. Cell Biol.* **8,** 633–644 (2007).
9. Sawyer, J. M. *et al.* Apical constriction: a cell shape change that can drive morphogenesis. *Dev. Biol.* **341,** 5–19 (2010).
10. Escudero, L. M., Bischoff, M. & Freeman, M. Myosin II regulates complex cellular arrangement and epithelial architecture in *Drosophila*. *Dev. Cell* **13,** 717–729 (2007).
11. Corrigall, D., Walther, R. F., Rodriguez, L., Fichelson, P. & Pichaud, F. Hedgehog signaling is a principal inducer of Myosin-II-driven cell ingression in *Drosophila* epithelia. *Dev. Cell* **13,** 730–742 (2007).
12. Vincent, A., Blankenship, J. T. & Wieschaus, E. Integration of the head and trunk segmentation systems controls cephalic furrow formation in *Drosophila*. *Development* **124,** 3747–3754 (1997).
13. Wang, Y.-C., Khan, Z., Kaschube, M. & Wieschaus, E. F. Differential positioning of adherens junctions is associated with initiation of epithelial folding. *Nature* **484,** 390–393 (2012).

14. Ghabrial, A., Luschnig, S., Metzstein, M. M. & Krasnow, M. A. Branching morphogenesis of the *Drosophila* tracheal system. *Annu. Rev. Cell Dev. Biol.* **19,** 623–647 (2003).
15. Oda, H. & Tsukita, S. Real-time imaging of cell-cell adherens junctions reveals that *Drosophila* mesoderm invagination begins with two phases of apical constriction of cells. *J. Cell Sci.* **114,** 493–501 (2001).
16. Campos-Ortega, J. A. & Hartenstein, V. *The Embryonic Development of* Drosophila melanogaster (Springer, 1997).
17. Lehner, C. F. & O'Farrell, P. H. Expression and function of *Drosophila* cyclin a during embryonic cell cycle progression. *Cell* **56,** 957–968 (1989).
18. Garner, M., van Kreeveld, S. & Su, T. T. *mei-41* and *bub1* block mitosis at two distinct steps in response to incomplete DNA replication in *Drosophila* embryos. *Curr. Biol.* **11,** 1595–1599 (2001).
19. Klämbt, C., Glazer, L. & Shilo, B. Z. *breathless*, a *Drosophila* FGF receptor homolog, is essential for migration of tracheal and specific midline glial cells. *Genes Dev.* **6,** 1668–1678 (1992).
20. Sutherland, D., Samakovlis, C. & Krasnow, M. A. *branchless* encodes a *Drosophila* FGF homolog that controls tracheal cell migration and the pattern of branching. *Cell* **87,** 1091–1101 (1996).
21. Baker, J. & Garrod, D. Epithelial cells retain junctions during mitosis. *J. Cell Sci.* **104,** 415–425 (1993).
22. Meyer, E. J., Ikmi, A. & Gibson, M. C. Interkinetic nuclear migration is a broadly conserved feature of cell division in pseudostratified epithelia. *Curr. Biol.* **21,** 485–491 (2011).
23. Bunch, T. A. *et al.* Characterization of mutant alleles of *myospheroid*, the gene encoding the β subunit of the *Drosophila* PS integrins. *Genetics* **132,** 519–528 (1992).
24. Leptin, M. & Grunewald, B. Cell shape changes during gastrulation in *Drosophila*. *Development* **110,** 73–84 (1990).
25. Martin, A. C., Kaschube, M. & Wieschaus, E. F. Pulsed contractions of an actin–myosin network drive apical constriction. *Nature* **457,** 495–499 (2009).
26. Martin, A. C., Gelbart, M., Fernandez-Gonzalez, R., Kaschube, M. & Wieschaus, E. F. Integration of contractile forces during tissue invagination. *J. Cell Biol.* **188,** 735–749 (2010).
27. Kato, K. & Hayashi, S. Practical guide of live imaging for developmental biologists. *Dev. Growth Differ.* **50,** 381–390 (2008).

**Supplementary Information** is available in the online version of the paper.

**Acknowledgements** We thank the Kyoto and Bloomington *Drosophila* Stock Centers, the Developmental Studies Hybridoma Bank, E. Wieschaus, H. Oda and T. Nishimura for fly stocks and antibodies; K. Kato and H. Wada for assistance with data analysis and experiments; G. Sheng, E. Kuranaga, K. Kato, T. Otani and B. Dong for comments on the manuscript; and members of the Hayashi, Nishimura and Kuranaga laboratories for discussions. This work was supported by Grant-in-Aid for Scientific Research on Innovative Areas (22111007 to S.H.); Grant-in-Aid for Young Scientists (B) (23770624 to T.K.) from The Ministry of Education, Culture, Sports, Science and Technology, Japan; and the RIKEN Special Postdoctoral Researcher Program (T.K.)

**Author Contributions** T.K. and S.H. conceived the project and wrote the manuscript, and T.K. performed the experiments.

**Author Information** Reprints and permissions information is available at www.nature.com/reprints. The authors declare no competing financial interests. Readers are welcome to comment on the online version of the paper. Correspondence and requests for materials should be addressed to S.H. (shayashi@cdb.riken.jp).

## METHODS

**Imaging.** Eggs were collected at 25 °C. Dechorionated embryos were mounted on a glass-bottomed dish (IWAKI) with glue and covered with water. Fluorescent images were captured by a confocal laser-scanning microscope (Olympus FV1000 with 15 mW laser diode 473 nm and 15 mW laser diode 559 nm lasers) with a ×60 oil immersion objective (PLAPON 60XO, numerical aperture 1.42, Olympus) at 25 °C. The confocal aperture was opened to 200 µm. Forty to sixty *z* stacks with a 0.7-µm interval were taken every 1–4 min for up to 300 min until the beginning of germband retraction. All the acquired images were smoothed with a 1-pixel-radius median filter and 1-pixel full-width at half-maximum Gaussian filter, and movements along the *x*–*y* position between time points were corrected by iSEMS[27]. The *y*–*z* or *x*–*z*-projected views were generated by software developed by K. Kato (unpublished software). '*xy*' shows the *Z*-projection view (except for Fig. 3b) and '*yz*' and '*xz*' show *X*-projection and *Y*-projection views of the boxed area in the '*xy*' view, respectively. In Supplementary Figs 1 and 8, '*yz*' and '*xz*' views are generated along the position of the mitotic cell. The apical area and depth of the apical surface were measured using Image J and calculated with Microsoft Excel. The depth of the tracheal pits was measured as the minimum length between the line of adherens junctions of the surrounding epidermal cells and the most internalized adherens junctions of tracheal pit as shown in Fig. 1b, inset. In Supplementary Fig. 8, the depth of the apical surface was measured as the minimum length between the line of PAR-6–GFP labelling of surrounding epidermal cells and that of each rounded cell (coloured). The developmental timing was determined in a variety of ways depending on the mutant conditions, as described in the figure legends. When obvious tracheal pits were observed (control, *CycA* and FGF-signalling mutants), the initiation of adherens junction depression at the centre was taken as time zero. Under conditions in which no clear tracheal pit formation was observed (EGFR-signalling mutants), the onset of germband retraction (initiation of the distance shortening between two adjacent tracheal pits) was set as time zero. In some cases, onset of the first mitosis 16 was set as time zero.

**Fly strains.** The following fly strains were used: *ubi-DE-cadherin-GFP* (*E-cad-GFP*)[15,28]; *histone H2Av-mRFP* (*His-RFP*)[29], *sqh-mCherry* (*myosin-mCherry*)[25], *par-6-GFP*[30], *UAS-mCherry-CAAX*[31] and *UAS-CycA*[32]. Information on the following stocks can be found in FlyBase (http://flybase.net/): $rho^{del1}$, $Egfr^{f24}$, $bnl^{P1}$, $btl^{\Delta Oh10}$, $CycA^{C8LR1}$, $dup^{a3}$, $snail^{IIG}$, $twist^{IIH}$, $mys^{XG43}$ and *1eve1 (trh-lacZ)*. $btl^{\Delta Oh24}$ is an imprecise excision mutant[33] from $btl^{6\text{-}81}$, in which a region including *btl*, *Fbp1* and *Sox21a* is deleted. In this study, $btl^{\Delta Oh10/\Delta Oh10}$ and $btl^{\Delta Oh10/\Delta Oh24}$ were used as *btl* mutants. We noticed that $btl^{\Delta Oh240/\Delta Oh24}$ mutant embryos showed the proper invagination movement, but could not initiate branching morphogenesis, the same as $btl^{\Delta Oh10/\Delta Oh10}$. Zygotic mutant embryos were distinguished using green balancers (*CyO, twi-GAL4 UAS-2xEGFP* or *TM3, twi-GAL4 UAS-2xEGFP*)[34]. Germline clones of $mys^{XG43}$ were generated in females of the genotype $mys^{XG43}$ *FRT19A*/$Ovo^{D1}$ *hsFLP FRT19A*; *ubi-DE-cad-GFP* and mated to *FM7a Dfd-GMR-YFP*/*Y*; *ubi-DE-cad-GFP* using the $Ovo^{D1}$ system[35]. Embryos that were negative for Dfd-GMR–YFP[36], were identified as maternal/zygotic *mys* mutant embryos. *ubi-GFP-CAAX* (membrane–GFP) and *trh66-GAL4* strains were generated by ΦC31-mediated transgene integration into attP target sites of the 22A or 86Fa strain[37] with the pUbi-GFP-CAAX and pGAL4-*trh66* plasmid, respectively.

**Plasmid construction.** All plasmids were constructed using PCR with PrimeSTAR (Takara Bio) and the In-Fusion PCR cloning kit (Clontech). For pUbi-attB, the promoter sequence of the ubiquitin gene[38] was amplified by PCR and used to replace the UAS enhancer and *hsp70* promoter region of pUAST-attB. In addition, the 3′ untranslated region (UTR) region of the ubiquitin gene was amplified by PCR from the genomic DNA of the Oregon R strain, and cloned into the KpnI site of the previously mentioned plasmid. The resulting plasmid was named pUbi-attB. For Ubi–GFP–CAAX, GFP fused with a 20-amino-acid carboxy terminal CAAX motif of human HRAS was amplified by PCR and cloned into NotI/KpnI-digested pUbi-attB. For pGAL4-attB, GAL4 was amplified by PCR and cloned into NotI/KpnI-digested pUAST-attB. Then the *hs43* promoter with the multi-cloning site of pCaSpeR-hs43-lacZ was amplified by PCR and cloned into the above plasmid digested with HindIII/NotI. The resulting plasmid was named pGAL4-attB. For pGAL4-trh66, the early trachealess enhancer (trh66)[39] was amplified from genomic DNA by PCR and cloned into KpnI/NotI-digested pGAL4-attB.

**Drug treatment.** Dechorionated embryos were treated with heptane for 5–10 s, and immediately washed with PBS containing 0.9 mM $CaCl_2$ and 0.5 mM $MgCl_2$ (PBS+). Embryos were mounted on a glass-bottomed dish (IWAKI) with glue and covered with PBS+, and fluorescent images were captured by a confocal laser-scanning microscope as already described. After mitosis 15, the covering PBS+ was replaced with PBS+ containing 50 mM or 500 mM colchicine, and time-lapse imaging was restarted. Only samples in which cells entered and were arrested at mitosis 16 were used for this analysis. (In the rest of the samples, the cells did not enter mitosis 16 and embryogenesis was arrested.)

**Laser ablation.** Laser ablation was performed using a confocal laser-scanning microscope (Olympus FV1000 with 15 mW laser diode 473 nm and 15 mW laser diode 559 nm lasers) equipped with an ultraviolet laser system (Olympus UV-ASU-P2) and a ×60 oil immersion objective (UPLSAPO 60XO, numerical aperture 1.35, Olympus). For fluorescent image acquisition, six *z* stacks with a 1-µm interval were taken every 3.53 s. Simultaneously with the image acquisition, a single pulse of a 349-nm laser (pulse duration <5 ns) was applied to cells at a specific time and defined depth. The area and depth of the cells were measured as described previously. A box plot was drawn using R software, showing the median as a line, the upper and lower quartiles as boxes, and the 1.5-interquartile range as whiskers. The *P* values were calculated using a Student's *t*-test (for two samples with similar variances, two-tailed) or Welch's *t*-test (for two samples with passively unequal variances, two-tailed).

**Immunohistochemistry.** Dechorionated embryos were fixed in 4% paraformaldehyde for 30 min at room temperature, and blocked with 0.1% bovine serum albumin, 0.2% Triton X-100 and 0.2% Tween-20 in PBS. The first antibody was diluted in the blocking solution and incubated overnight with gentle rotation at 4 °C. After washing, the second antibody, diluted in the blocking solution, was added, and the tissue was further incubated for 2 h at room temperature. After washing, the embryos were mounted in Vectashield mounting medium with 4′, 6-diamidino-2-phenylindole (DAPI, Vector Laboratories) and photographed using an Olympus FV1000 confocal microscope with a ×20 objective lens (UPLSAPO 20X numerical aperture 0.75, Olympus) and a ×60 water immersion objective lens (UPLSAPO 60XW numerical aperture 1.2, Olympus). The following antibodies were used: mouse anti-β-galactosidase (1:100, 40a-1, DSHB), rabbit anti-β-galactosidase (1:1,000, Cappel), rabbit anti-DsRed (1:5,000, BD Biosciences), rat anti-DEcad (1:20, DSHB), anti-mouse IgG Alexa 488 (1:500, Molecular Probes), anti-rabbit IgG Alexa 555 (1:500, Molecular Probes) and anti-rat IgG Dylight649 (1:500, Jackson Laboratory).


28. Haruta, T., Warrior, R., Yonemura, S. & Oda, H. The proximal half of the *Drosophila* E-cadherin extracellular region is dispensable for many cadherin-dependent events but required for ventral furrow formation. *Genes Cells* **15,** 193–208 (2010).
29. Pandey, R., Heidmann, S. & Lehner, C. F. Epithelial re-organization and dynamics of progression through mitosis in *Drosophila* separase complex mutants. *J. Cell Sci.* **118,** 733–742 (2005).
30. Wirtz-Peitz, F., Nishimura, T. & Knoblich, J. A. Linking cell cycle to asymmetric division: Aurora-A phosphorylates the par complex to regulate numb localization. *Cell* **135,** 161–173 (2008).
31. Kakihara, K., Shinmyozu, K., Kato, K., Wada, H. & Hayashi, S. Conversion of plasma membrane topology during epithelial tube connection requires Arf-like 3 small GTPase in *Drosophila*. *Mech. Dev.* **125,** 325–336 (2008).
32. Hayashi, S. & Yamaguchi, M. Kinase-independent activity of Cdc2/Cyclin A prevents the S phase in the *Drosophila* cell cycle. *Genes Cells* **4,** 111–122 (1999).
33. Ohshiro, T. & Saigo, K. Transcriptional regulation of *breathless* FGF receptor gene by binding of TRACHEALESS/dARNT heterodimers to three central midline elements in *Drosophila* developing trachea. *Development* **124,** 3975–3986 (1997).
34. Halfon, M. S. *et al.* New fluorescent protein reporters for use with the *Drosophila* Gal4 expression system and for vital detection of balancer chromosomes. *Genesis* **34,** 135–138 (2002).
35. Chou, T. B. & Perrimon, N. Use of a yeast site-specific recombinase to produce female germline chimeras in *Drosophila*. *Genetics* **131,** 643–653 (1992).
36. Le, T. *et al.* A new family of *Drosophila* balancer chromosomes with a $w^-$ dfd-GMR yellow fluorescent protein marker. *Genetics* **174,** 2255–2257 (2006).
37. Bischof, J., Maeda, R. K., Hediger, M., Karch, F. & Basler, K. An optimized transgenesis system for *Drosophila* using germ-line-specific φC31 integrases. *Proc. Natl Acad. Sci. USA* **104,** 3312–3317 (2007).
38. Lee, H. S., Simon, J. A. & Lis, J. T. Structure and expression of ubiquitin genes of *Drosophila melanogaster*. *Mol. Cell. Biol.* **8,** 4727–4735 (1988).
39. Sotillos, S., Espinosa-Vázquez, J. M., Foglia, F., Hu, N. & Hombría, J. C.-G. An efficient approach to isolate STAT regulated enhancers uncovers STAT92E fundamental role in *Drosophila* tracheal development. *Dev. Biol.* **340,** 571–582 (2010).